International Journal of Bioelectromagnetism *www.ijbem.org*
Vol. 12, No. 3, pp. 133 - 151, 2010

Anatomic Reentry: Insights from a Parametric Study on a Simple 3D Anisotropic Wedge Model

Mihaela Pop[a], Maxime Sermesant[b,c], Jean-Marc Peyratt[b,d], Eugene Crystal[a], Alexander J Dick[a], Graham A Wright[a]

[a]*Sunnybrook Health Sciences Centre, University of Toronto, Canada*
[b]*INRIA - Asclepios project, Sophia Antipolis, France*
[c]*Division of Imaging Science, King's College Hospital, London, UK*
[d]*Simens Molecular Imaging, Oxford, London,UK*

Correspondence: Mihaela Pop, Dept. of Medical Biophysics, University of Toronto, 2075 Bayview Ave., Sunnybrook Research Institute, Toronto, M4N 3N5, ON, Canada. E-mail: mihaela.pop@utoronto.ca, phone +01 4164806100, fax +01 4164805714

Abstract. In patients with prior chronic myocardial infarct, some anatomic circuits formed by scars can create reentrant waves which lead to ventricular tachycardia (VT), a dangerous high heart rate. The purpose of this work was to investigate via computer modelling how the myocardial conductivity and anisotropy of myocardium affect the creation of unidirectional blocks (UB) and, further, the inducibility of reentry as well as the VT cycle length. The simulations were produced for a realistic 3D wedge of ventricle (3.4x3.4x1.5cm) with realistic fiber orientations included. For a given anatomic circuit, we define electrically inert scars, encasing a channel (named the isthmus) of slow conduction. We show that the VT cycle length corresponding to the re-excitation of the tissue due to a fast looping of a reentrant wave around the scars, is directly proportional to the square root of the isthmus conductivity (with curve fitting yielding a correlation coefficient of 0.99). We used the model to assess the re-inducibility of VT following placement of ablation lesions in the isthmus. We show that incomplete ablation of the principal isthmus of existing VT is not enough to stop the reentrant wave. Furthermore, if a secondary isthmus exists, the resultant wave may take a shorter path through this secondary isthmus to yield different VT.

Keywords: Cardiac Electrophysiology, Anatomic Reentry, Computer Model, Rafiofrequency Ablation

1. Introduction

Sudden cardiac death is frequently a lethal complication for patients with prior myocardial infarction and is an outcome of arrhythmic events [Huikuri *et al.*, 2001]. Changes in the structural and electrophysiological properties of the myocardium during healing in the infarct and surviving peri-infarct (border-zone) areas are known to contribute to arrhythmogenesis [Kleber and Rudy, 2004]. An important pathophysiologic substrate of ventricular arrhythmias is *reentry*, an abnormal re-excitation of the myocardium which can cause the heart to beat at very rapid and potentially lethal rates [Martinez-Rubio *et al.*, 1999]. The mechanism of reentry can be either *functional* or *anatomic* in nature [Garratt, 2001]. The former can be induced in excitable tissue without structural barriers but with altered refractory properties due to ischemic conditions and is more common in the acute phase of the infarct [Janse and Wit, 1989]. On the other hand, an *anatomic reentry* requires the presence of structural obstacles (e.g. infarct scars, pulmonary veins) that block the impulse conduction since they are electrically inert [De Bakker *et al.*, 1993, Kawara *et al.*, 2001]. There is abundant evidence demonstrating that some bundles of muscle survive the infarct episode and, together with fibrotic bundles, create channels encased between the dense scars [Peters and Wit, 1998]. The deposition of fibrosis changes local myocardial structure and architecture, and is accompanied by cellular electrical uncoupling and gaps closure [Spach and Josephson, 1993]. This results in a decrease of conduction velocity (CV), and thus a slower propagation of the action potential (AP) through the channels (called *isthmuses*). The conduction velocity of the excitation wave depends on the electro-diffusion, which is tuned by the ionic conductivities in the intra- and extra-cellular spaces. The diffusion term is generally

referred to as 'conductivity' [Ten Tusscher and Panfilov, 2007; Jie *et al.*, 2008] and it is assumed that the CV of a planar excitation wave through myocardium varies with the square root of this (apparent) bulk conductivity. Furthermore, the AP wave front propagates faster in the longitudinal direction (parallel to the fibers) leading to an anisotropic propagation of the wave front.

Correlation between electrophysiological and structural changes is of great importance as such changes are known to become a substrate of ventricular tachycardias (VT) [Bolick *et al.*, 1986]. Experimental and clinical studies have demonstrated that the VT cycle length (the time between two consecutive reentrant waves) depends on: how slowly the electrical wave propagates through the isthmus and around the scars; myocardial anisotropy; and the physical dimensions of the conduction blocks [Pogwizd *et al.*, 1992; Ciaccio *et al.*, 2001; Soejima *et al.*, 2002; Girouard *et al.*, 2001]. Via voltage mapping techniques, it has been shown that clinically relevant anatomic reentries are *macro-reentries*, which can be fairly large in humans, with isthmuses up to a few centimeters in width and length [De Chillou *et al.*, 2002].

Anatomic circuits (as illustrated in Fig 1a) have five components: i) unexcitable scars (*S*); ii) outer pathways of healthy tissue; (iii) the isthmus (*I*) of reduced conductivity; (iv) an entrance site located at one end of the isthmus; and (v) an exit site located at the other end of the isthmus (the arrows show the direction of wave propagation around the scars).

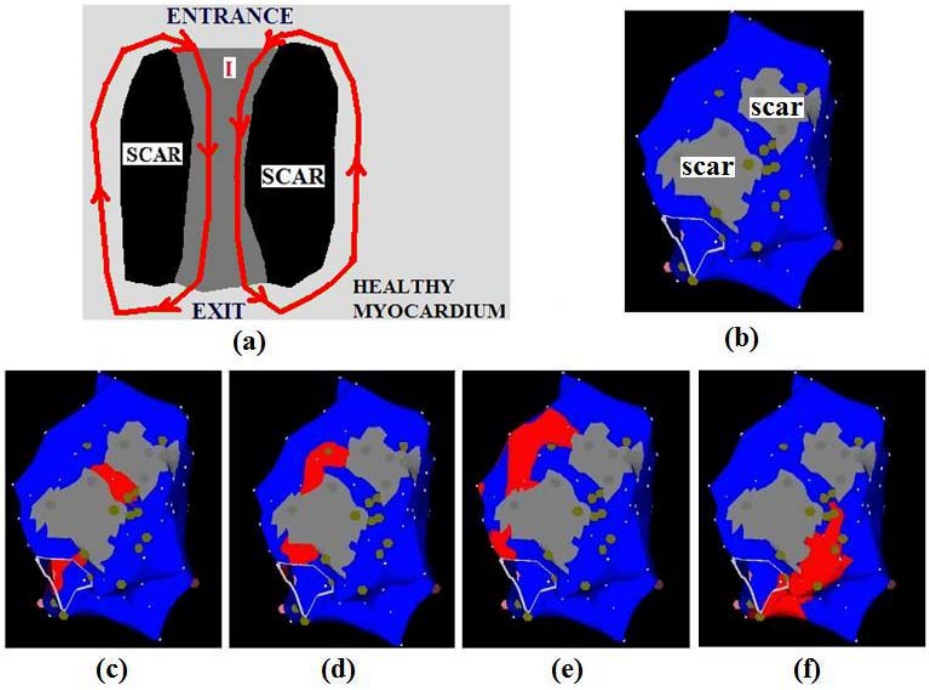

Figure 1. *Anatomic reentry: (a) schematic diagram of a reentrant circuit and (b-f) example of reentrant wave propagation around the scars in a VT patient (images kindly provided by the Catheter Lab, Arrhythmias Services, Sunnybrook Health Sciences Centre, Toronto, Canada). The activation front of the wave (in b-f) is represented in red, normal myocardium is in blue and the scars are in grey (note that the isthmus allows the propagation of wave whilst the scars block the wave and force it to loop around this anatomic circuit).*

An example of surfacic measured data in a VT patient, obtained with the CARTO electro-anatomic mapping system (BiosenseWebster, Johnson&Johnson) after identification of scars and VT induction (unpublished data, CARTO images courtesy of Catheter Laboratory, Arrhythmias Services, Sunnybrook Health Sciences Centre, Toronto, CA) is given in Fig 1 b-f (with the scar in gray, normal myocardium in blue and depolarization wave front in red). The white dots represent the interrogation (measurement) points. Notice that in the snapshot shown in Fig 1c the wave travels right through the isthmus, then exits the circuit (Fig 1d) and starts to loop around the scars (Fig 1e-f).

Currently, the attempts to characterize reentrant circuits and their VT cycle length are limited to data measured based on endo and / or epicardial mapping, during sinus rhythm, moderate pacing and sometimes on high output stimulation. Unfortunately, the electrical measurements obtained during the

electrophysiology (EP) procedures are recorded at a low spatial resolution (4-5mm), and fail to identify reentries deep in the myocardium. Moreover, the clinical protocol to induce VT is invasive and requires pacing the heart at high rates, where VT can degenerate into ventricular fibrillation (a fatal disorganized and asynchronous cardiac excitation). The measurements are taken from different locations by applying multiple extra stimuli delivered in decreasing time steps such that one stimulus will reach the circuit and initiate VT; this results in extremely long procedures [Stevenson *et al.,* 1993, Ciaccio *et al.,* 2003]. However, poor identification of reentrant circuits limits the success of radio-frequency RF ablation, the only curative therapy that can effectively interrupt the reentry circuits by creating small, continuous, thermal lesions in the isthmus [Kottkamp *et al.,* 2003]. Moreover, gaps within an RF lesion or the presence of bystanders (secondary isthmuses, which are "silent" prior to ablation) are suspected to be the cause of initial monomorphic VT re-inducibility with a new morphology. Therefore, better understanding of the interrelation between the intrinsic physical properties of the circuit (conductivity, geometry, anisotropy) as well as prediction of VT inducibility and estimation of the cycle length for each circuit is very important. There is a clear need to supplement the EP measurements with mathematical characterization; manual calculation can be useful [Stevenson *et al.,* 1989] but is limited to 2D calculations due to the surfacic nature of measurements. Thus, theoretical models yielding fast 3D characterization may become an important non-invasive tool for guiding RF ablation of re-entrant VT.

Computer modelling has been intensively used in the past decade as a non-invasive electrophysiology tool. Of particular interest are parametric studies which can estimate behavior that is difficult to measure experimentally. Simple and complex models have been proposed to simulate the electrical activity of the normal or pathologic heart and to predict its behavior under different treatment scenarios; their utility was reviewed recently [Clayton and Panfilov, 2008]. The complexity of computer models depends on the model scale, and is often limited by available computer resources. Most importantly, the models have to be versatile and accurate enough for the purpose of a given study. For example, the majority of the functional reentries and fibrillation-related phenomena are studied using cellular ionic models [Noble, 1962; Luo and Rudy, 1994, Bernus *et al.,* 2002; Clayton and Holden 2003; Benson *et al.,* 2007] as well as bidomain equations [Jie *et al.,* 2008, Trayanova, 2008], the latter model explicitly solving for extracellular and intracellular voltages. The ionic models employ a large number of variables and equations as they calculate the transmembrane potential for each cardiac cell, making them computationally expensive and difficult to integrate into a clinical therapy platform. Therefore, most of these computations are carried out on supercomputers and parallel clusters [Xie *et al.,* 2004; Potse *et al.,* 2006]. Other models, like the phenomenological model proposed by FitzHugh-Nagumo (FH-N), use a simple reaction-diffusion system of equations to compute the propagation of AP without computing individual ionic currents [FitzHugh 1961, Nagumo *et al.,* 1962]. This model was found useful by Friedman and collaborators [2004] to observe wave propagations in response to different stimulating pulses that could identify the reentry in excitable tissues (in 1D and 2D simulations), as well as in [Krogh-Madsen and Christini, 2008] who studied the conditions for re-setting and/or terminating reentry following application of stimuli at different distances from the circuit. The monodomain model was also found suitable for studying the propagation of AP waves in tissues with electrically inert scars (due to fibrosis). Such efforts include 1D and 2D simulations produced in [Kogan *et al.,* 1992] to study the mechanism of unidirectional block, UB (i.e., a conducting portion of tissue that provides a retrograde pathway for the propagating pulse) in narrow channels, and by Sinha and collab. [2002a, 2002b], who proposed pacing algorithms at different frequencies in order to annihilate the anatomic reentrant waves. In addition, the FH-N model was also used to simulate the 2D and 3D propagations of excitation and anchoring of spiral waves in the presence of large unexcitable obstacles [Ten Tusscher and Panfilov 2003, 2005, 2007]. Other authors [Sermesant *et al.,* 2003, 2005, 2006] implemented this formalism to a 3D electro-mechanical model heart, with an aim to test and integrate fast cardiac models into clinical applications. We have recently used this model proposed by Sermesant and collaborators, and developed a simple 3D theoretical model (based on the FH-N formalism) that predicts VT inducibility in the presence of macro-reentry circuits [Pop *et al.,* 2008]. We mimicked an isthmus (4 mm width, 1.8 cm length and variable cross-section) encased by two unexcitable scars (1.8x0.7cm each). These results demonstrated on a simplistic rectangular slab (2.5x2.5x1cm; 1 mm element size) that VT cycle length depends directly on the conduction velocity, which in turn depends on the isthmus conductivity and cross-section of the isthmus, as well as myocardial anisotropy. However, this model was limited in that the fiber orientations were unrealistic (i.e., all fibers were assigned in vertical direction and parallel through the slab) and the slab was a rectangle.

Our goal is to better understand the impact of model variables on critical reentry characteristics. Thus, in the present study, we use the same mathematical model but we explore a more realistic situation, simulating anatomic reentries on a 3D wedge of ventricular tissue, with fiber directions obtained from diffusion-weighted MR imaging. Via computer simulations, we studied the propagation of the cardiac action potentials in the presence of a simple macro-reentry epicardial circuit, with electrical waves circulating around two large obstacles (i.e. infarct scars). We specifically identify the lower and upper limits of the vulnerable window (VW) which correspond to a unidirectional block (UB) condition in the isthmus. We then examine how the width of VW and the VT cycle length are modified after we systematically change the: i) myocardial anisotropy ratio (i.e., the ratio between transverse and longitudinal conduction velocities) and ii) conductivity values in the isthmus. In addition, we alter the circuit geometry by placing virtual RF ablation lesions on the isthmus (including the presence of a gap in an RF ablation lesion, as well as the presence of a bystander isthmus) and investigate the effects on the VT cycle length.

2. Material and Methods

2.1. Theoretical considerations

At a macroscopic level, the predictions of action potential (AP) propagation can be achieved by solving the reaction-diffusion equations originally developed in [FitzHugh, 1961] and [Nagumo, 1962]. To correct for the after-hyperpolarization phase specific to nerve axons, Aliev and Panfilov [1996a] modified this model and proposed the following equations (1-2) for cardiac tissue:

$$\frac{\partial V}{\partial t} = \nabla \cdot (D \nabla V) - kV(V - a)(V - 1) - rV + I_{stim} \quad (1)$$

$$\frac{\partial r}{\partial t} = -(\varepsilon + \frac{\mu_1 r}{\mu_2 + V})(kV(V - a - 1) + r) \quad (2)$$

where: the two dimensionless variables are *V*, the transmembrane potential, and *r*, the recovery variable contribution (the latter determines the dynamics of the recovery phase of the action potential). Extra stimuli can be introduced at any instant into the tissue and are represented by the term I_{stim}. The term $-kV(V-a)(V-1)$ controls the fast processes (initiation and upstroke of action potential) via the threshold parameter, *a*; ε^{-1} is a time constant for the recovery phase. The reaction and recovery parameters involved in this two-variable model (i.e., $a = 0.1$, $\varepsilon = 0.01$, $k = 8$, $\mu_1 = 0.1$ and $\mu_2 = 0.3$) were introduced in [Nash and Panfilov, 2004]. The resulting action potentials reproduce the shape, duration, refractoriness and restitution of action potentials obtained in [Elharrar and Surawicz, 1983] from experiments in canine cardiac tissue. The variables in this model are dimensionless; but they can be re-scaled to be related to physical values. For example, the normalized AP in the model varies between 0 and 1, which corresponds to real values between -90 and +20 mV.

The Aliev-Panfilov model accounts for tissue anisotropy via the conductivity (diffusivity) tensor, D, and can be written as $D = d_0 \cdot \mathrm{diag}(1, \rho, \rho)$ in the local orthonormal basis (*i*,*j*,*k*), where *i* is the direction parallel to the fiber, ρ is the ratio between the transverse and the axial conductivities and d_0 is the normalized scalar conductivity (which is set to 1 for healthy tissue). Note also that for a planar wave, a simple analytical relationship between CV and the diffusivity *d* can be written: $CV \propto (d)^{1/2}$ [Keener and Sneyd 1998]. Typically, the waves propagate approximately twice as fast in the direction parallel to the fibers relative to the transverse direction. Therefore, we expect an anisotropic ratio $CV_{transv} : CV_{longitud}$ of approximately 1:2. In our current study, the effects of anisotropy were observed by varying the tissue anisotropy ratio which corresponded to gradually reducing the transverse CV (e.g. a ratio of 1:1 corresponds to an isotropic case; for 1:2 the wave propagates twice as slow in the transverse direction and corresponds to $\rho = 0.25$; for 1:3 the wave propagates three times slower in the transverse direction and corresponds to $\rho = 0.11$).

2.2. Wedge model preparation and computer model implementation

Figure 2 shows the preparation of the 3D wedge model from a porcine heart scanned for fiber orientation using diffusion-weighted MRI. Details of the DW-MRI scanning parameters can be found

in [Pop *et al.*, 2009a]. The in-plane spatial resolution for this particular scan was 0.4x0.4mm and the slice thickness was 1.5mm; 7 diffusion directions were acquired.

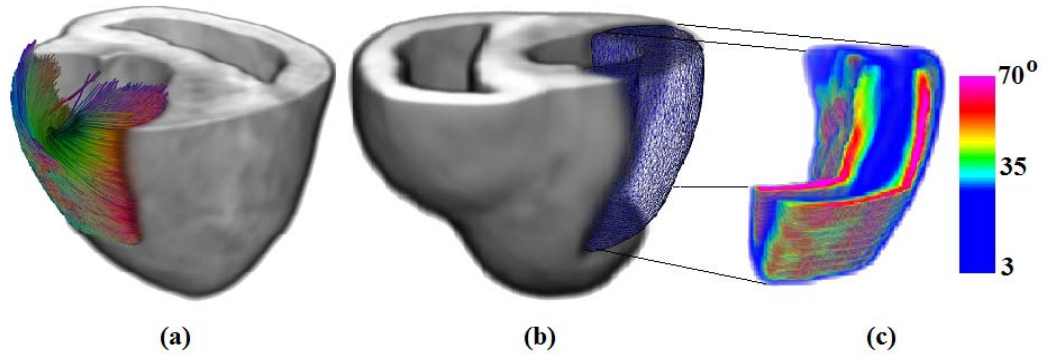

Figure 2. *The wedge model obtained from a porcine heart: (a) the orientation of bundles derived from diffusion-weighted MRI acquisitions are shown as colored lines, demonstrating the expected rotation across the ventricle wall; (b) the 3D anatomical model is shown in gray; (c) corresponding tetrahedral mesh of the wedge is shown in blue and rotation angle of the fibers from the epicardium to the endocardium through the wedge is depicted as a color scale (cut-away lateral view).*

To illustrate propagation behavior for a particular pattern of myocardial damage we then defined zones in the mesh, particularly the scars and the isthmus creating a specific circuit geometry (Fig 3a and 3b depict the frontal view and cross-section, respectively). Furthermore, we assigned fiber directions to each vertex in the mesh. The electrically inert scars were approximately 22 mm in length and 8 mm in width (as measured on the epicardium) encasing an isthmus 5 mm wide with a cross-sectional area of approximately 15mm^2. We assigned zero conductivity to the transmural scar, and a reduced d_0 to the isthmus; we also changed the anisotropy ratio to reflect the fiber directions. Variation in the electrical conductivity was obtained by changing the value of d_0 incorporated in the diffusion term of equation (1).

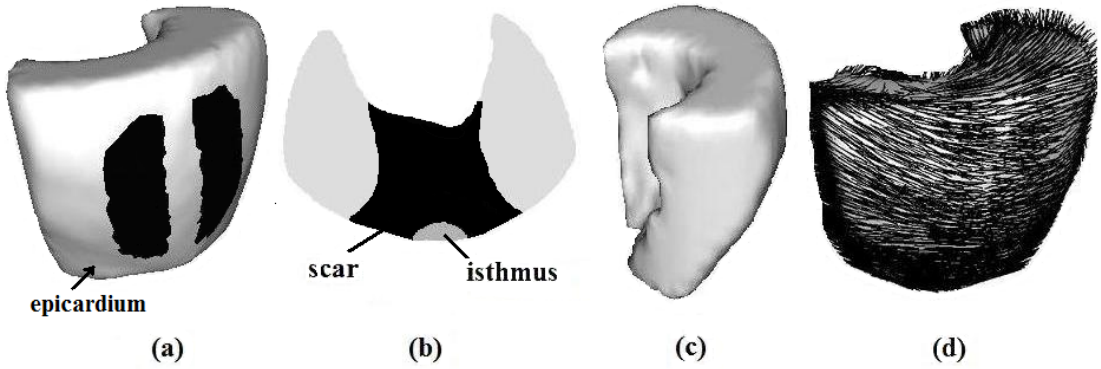

Figure 3. *The resulting 3D model after the wedge (light grey) is cropped and the infarct areas (in black) as well as the isthmus are defined: (a) frontal (anterior) view; (b) cross-section view; and (c) lateral view of the anatomical model of the wedge, respectively; (d) the fiber directions assigned to each node in the mesh.*

We solve for the transmembrane potential over a computational mesh of 61600 elements generated with the GHS3D package (INRIA, France) for the wedge model. The code is written in C++ and uses OpenGL libraries to display the results. We employed Finite Element Methods, using an explicit forward Euler time integration scheme. We imposed Neumann no-flux boundary conditions at all tissue boundaries, i.e. $\hat{n} \cdot (D\tilde{N}V) = 0$, where $\hat{n}$ is the unit vector normal to the boundary. For the simulations presented in this study, we used a computational time step of 5x10^{-5}s. The time step was determined from convergence tests, such that further refinement did not significantly change the solution for transmembrane potential. The simulation time for one heart cycle of 0.7s on this mesh is about 40 min on an Intel ® Pentium 4, 3.2GHz CPU, with 1GB of RAM.

2.3. Electrophysiological considerations of anatomic reentry

In order to induce reentrant activity, certain fundamental conditions must be satisfied including: 1) the presence of a heterogeneous anatomic circuit with a geometry defined by unexcitable obstacles (i.e., scars forcing the electrical wave to propagate around them); and 2) a premature stimulus to initiate a perturbation in the normal electrical propagation through the given circuit, triggering a unidirectional conduction block (UB) through the isthmus of slow conduction [Garratt, 2001]. The extra stimulus S2 has to arrive within a specific time interval, called vulnerable window (VW). We systematically changed the conductivity of isthmus and anisotropy ratio of the myocardium, analyzing the effect of these variables on the creation of UB and its associated VW. The perimeter of the scar and the conduction velocity of the outer and inner segments of the circuit determine the VT cycle length.

2.4. Simulations on the 3D wedge

We first calculated the propagation of action potential, AP, on the 3D wedge representing ventricular tissue (Figure 3a). The majority of the macro-reentry circuits (mapped in animals and humans) have areas reported on the order of a few cm^2, with the narrowest width of clinically significant isthmuses being on the order of a few millimeters [Ciaccio *et al.,* 2001, Soejima *et al.,* 2002, De Chillou *et al.,* 2002]. Therefore, the size of the wedge (i.e., 3.5 x 3.5 x 1.5 cm) and the tetrahedral mesh (about 1-1.2 mm element size) were chosen to enable realistic characterization of macro-reentry circuits in a reasonable computational time for a fine mesh.

The wedge was paced at constant 700 ms interval, via a stimulus S1 (e.g. a square pulse of maximum AP amplitude) applied at the bottom of the wedge, mimicking a wave propagating in the apex-to-base direction, after pacing the heart at the apex. In equations (1) and (2), this is accomplished via the initial conditions; that is, we set artificially the voltage V=constant, at maximum amplitude (V = 1) for 10 ms to the entire surface of the bottom of the wedge. The stimulation pulse initiates a depolarization wave that propagates from the bottom towards the top of the wedge. As per the requirements described in Section 2.3, we also applied one extra stimulus S2 (5 ms duration) of maximum amplitude (i.e., AP = 1) close to the entrance of the isthmus (on an area of approximately $10mm^2$), with a coupling interval S1-S2 which was varied until we achieved unidirectional block, UB, through the isthmus, initiating the VT reentrant waves. We varied the conductivity in the isthmus as well as the anisotropy ratio and measured the VT cycle length. Linear fitting was performed in Excel to derive the relationship between these variables. An additional example is also included, illustrating an endocardial scar with an isthmus (4 mm wide and 18 mm long) traversing the scars (6 mm in width, as measured on the endocardium). The conductivity of the isthmus was set to $0.5*d_0$, whereas the anisotropy ratio was set to 1:2.

Throughout this current study, we set the longitudinal conduction velocity to a value of 25cm/s. This choice was due to the small size of the scars and conditions to induce VT (see **2.3.**). We have demonstrated in our previous study [Pop *et al.,* 2008] that, in the setting of a relatively small scar, the time required for a reentrant wave to complete a rotation had to be longer than APD; otherwise the head of the reentrant wave will encounter refractory tissue and cannot propagate. This time is equal to the ratio between the perimeter of the scar and the speed of propagation; thus, for a circuit of given size, there is a maximum value for speed we could use to simulate the wave propagation.

To mimic a failure of the RF ablation therapy, we placed electrically inert RF ablation lesions along the isthmus where we set the conductivity to zero (as the lesions block the propagation of electrical waves). We designed circuits with gaps in the lesion, through which the reentry wave could escape and continue to propagate and investigated the effects on the VT cycle length. We also introduced a secondary isthmus within the scars (named a bystander) that forces the wave to circulate through a shorter path after ablation.

3. Results

3.1 Unidirectional block on the isthmus and inducibility of reentrant VT

We first present an example (see Fig. 4) corresponding to a situation where the unidirectional block is successfully generated and the reentry is induced. A pacing stimulus S1 is applied for 10 ms

starting at t = 0 and, as a result, the depolarization wave (in red) propagates from the bottom of the wedge to the top, as seen in Figs 4a-b, both at time t = 0.01 s. The propagation is perturbed due to the presence of the infarct scars (in black) which are electrically inert. The conductivity in the isthmus was reduced by 50% relative to the conductivity of normal myocardium. As a result, the depolarization wave propagates through the healthy tissue, around the scars, and more slowly through the isthmus than through the normal tissue (Fig 4c, at t = 0.11 s). This is followed by a repolarization phase of the tissue, as shown in the corresponding snapshots in Fig 4d at t = 0.23 s, and Fig 4e at t = 0.37 s, respectively. The red represents an activated state of tissue; blue corresponds to the resting state; and yellow corresponds to the re-polarization phase.

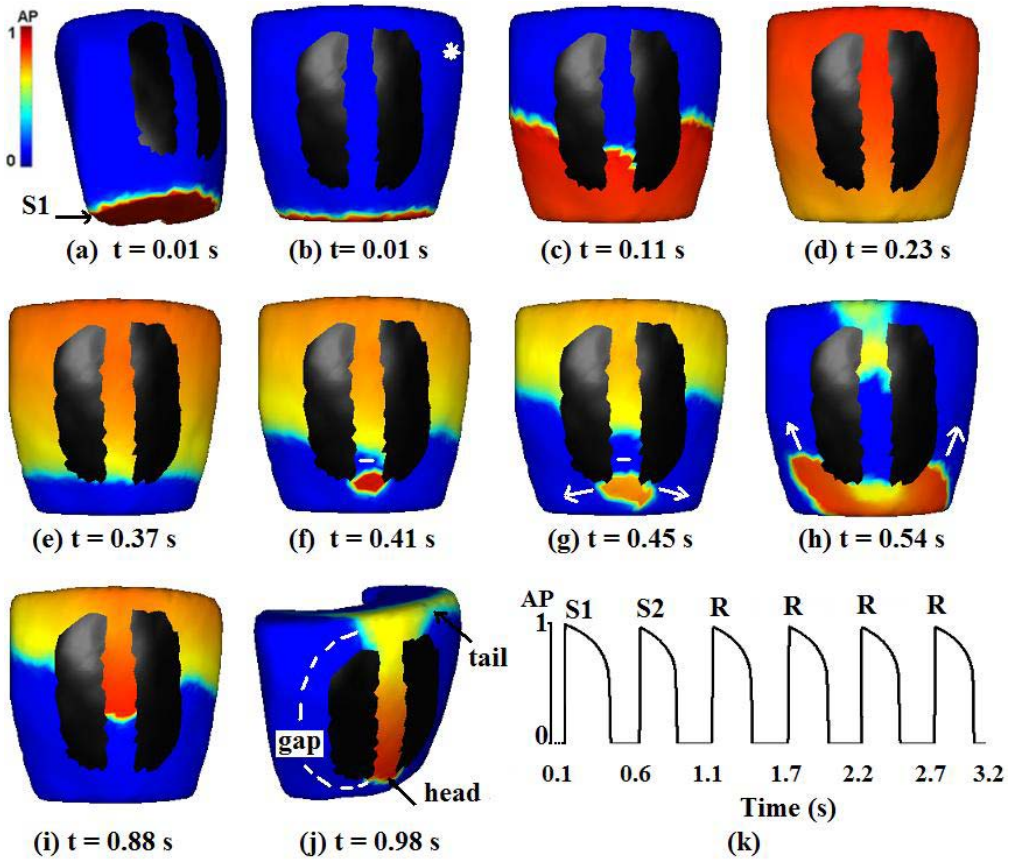

Figure 4. *Inducibility of epicardial reentry: the stimulus S1 initiates the electrical excitation from the bottom of the wedge as seen in (a) tilted lateral view and (b) frontal view, and propagates through the tissue, with the red and blue colors representing the depolarized and rest phases of action potential AP respectively, and the yellow corresponding to the repolarization phase. Snapshots (c-j) correspond to the propagation of a depolarizing wave, creation of unidirectional block and the initiation and perpetuation of reentry through the isthmus where the conductivity was reduced by 50% relative to the normal tissue. White arrows indicate the direction of wave propagation whilst the white bar (f) indicates that the wave stops when it encounters refractory tissue following application of the extra-stimulus S2 (at one end of the isthmus). A 'diastolic gap' is defined by the head and the tail of the reentrant wave (j). The traces (in k) correspond to the changes in AP simulated over the first 3 seconds (where R-R-R… denotes reentrant waves generated in response to the S2 stimulus), measured at the location given by the white asterisk seen in (b).*

An extra stimulus S2 is applied for 5 ms when the isthmus is still refractory (e.g. 190 ms before the next S1 would be applied); this creates a unidirectional block (UB) in the isthmus because this stimulus arrives at a time before the isthmus can conduct the impulse (that is at t = 0.41 s in Fig 4f), whereas the healthy tissue has recovered and can conduct the electrical impulse (Fig 4g-h, snapshots taken at t = 0.45 s and 0.54 s respectively). Thus, the initiated wave propagates around the scars and enters the isthmus from the opposite end (Fig. 4i, at t = 0.88 s). The wave then propagates through the isthmus in a retrograde direction, from the top to the bottom, creating a reentry.

The tissue between the head of the wave (defined by the excitation front) and the tail of the wave is always refractory; however there is a so-called 'diastolic gap' between the tail and the head, where tissue has recovered and is excitable (Fig 4j, taken at t = 0.98 s). The resulting VT cycle length is given by the time between two consecutive excitations (R-R) at a given point in the circuit (indicated by the white asterisk in Fig 4b). Multiple heart cycles are shown over 3s in Fig 4k, for which we calculated a VT cycle length of 526 ± 13 ms (mean ± SD). The fibers' orientation relative to the anatomic circuit can be observed in Fig. 8b. Variations in anisotropy ratio explored in the paper were obtained by reducing the transverse CV (see section **2.1** for details).

The interval between S1 and S2 (known as the 'coupling interval') is a critical parameter in the creation of unidirectional block (UB); we gradually reduced this interval by time steps of 20 ms, 10 ms, 5 ms, 2 ms and 1 ms, until we obtained UB. Figure 5 includes simulation results when the S2 is applied either below a lower limit when the isthmus and the healthy tissue are still refractory and the new excitation wave extinguishes (Fig 5a-b) or above an upper limit when the isthmus has recovered and thus the wavefront can propagate in all directions (Fig.5c-d). However, when S2 is applied any time between the lower limit and the upper limit, the UB is generated, as observed in Fig 5e-f. These two limits define a vulnerable window (VW), which is a characteristic time interval of each anatomic circuit. For the example given in Fig 5 (obtained when the conductivity in the isthmus was reduced by 50% relative to that of normal conductivity, and the anisotropy ratio was set to 1:2), the VW was found to be between 349 ms and 396 ms after S1. Any extra stimulus (S2) applied outside this time interval (either before or after) did not create a unidirectional block.

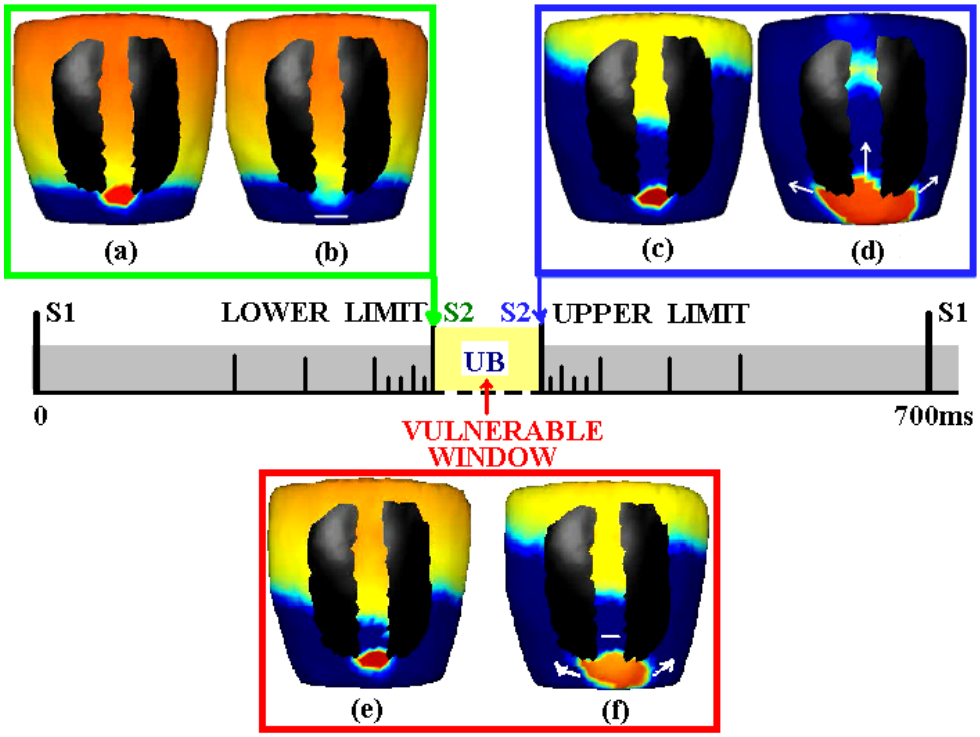

Figure 5.*(a-f) Lower limit of VW in green panel (a-b) and upper limit, respectively, in blue panel (c-d) associated with the S1-S2 coupling interval that does not induce UB. S1-S2 is progressively reduced, until S2 induces UB (e-f). White arrows indicate the direction of wave propagation and white bars indicate that the wave stops when it encounters refractory tissue.*

The lower and upper limits of the VW (corresponding to UB) as a function of conductivity of the isthmus and myocardium anisotropy, respectively, are shown in Fig 6 (a-b); these results were obtained using the fiber directions as displayed later in Fig 8b. Specifically, we first set the anisotropy ratio to 0.25 (i.e., the ratio between CV_{transv} and $CV_{longitud}$ is 1:2), and varied the conductivity of the isthmus relative to that of normal myocardium; we established the lower and upper limits of VW by changing the S1-S2 interval. From Fig 6a, the width of the VW (when the UB is created) increases from to 17 ms to 55 ms as conductivity in the isthmus decreases from 1.0 to 0.15 (relative to normal myocardium). There is a small shift (10 ms) in the values corresponding to the lower limit (i.e., from 340 ms to 350 ms) and a larger shift (46 ms) in the upper limit (i.e., 357 ms from to 403 ms) of the interval S1-S2, as

the conductivity in the isthmus decreases. In Fig 6b we set the conductivity of the isthmus to be 75% smaller than that of normal myocardium, and varied the anisotropy ratio. The results presented in Fig 6b demonstrate that the width of the VW increases when the anisotropy increases. Notice that the lower limits shifted earlier (i.e., from 360 ms in the isotropic case to 341 ms for conduction velocity ratio of 1:3); thus the UB was created earlier. The upper limit did change substantially as the ratio between CV_{transv} and $CV_{longitud}$ went from 1:1 to 1:2 (i.e., anisotropy ratio went from 1 to 0.25), but changed little with greater anisotropy.

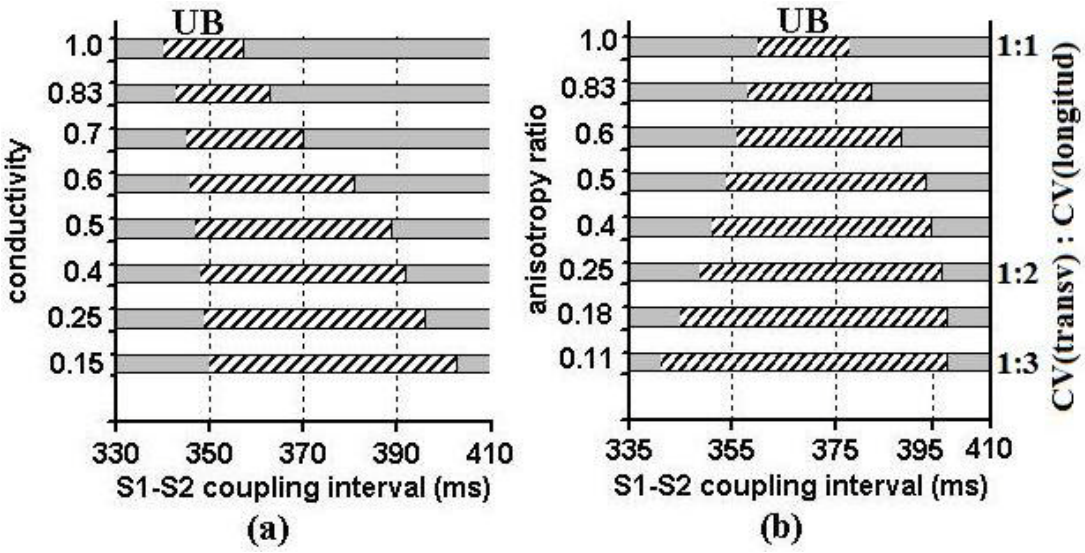

Figure 6. *Lower and upper limits, of the VW corresponding to the creation of the UB (dashed areas). The S1-S2 coupling interval is plotted as function of conductivity of the isthmus (a) and myocardial anisotropy (b), respectively. Grey shades correspond to the times outside the VW, for which UB cannot be created.*

3.2. The effect of isthmus conductivity and myocardial anisotropy on VT cycle length

Figures 7(a-c) illustrate differences in the propagation of the wave front through the isthmus when the conductivity of the isthmus is reduced by (a) 75%, (b) 40% and (c) 12%, respectively. The snapshots were taken at the same time (i.e., t=0.157s after S1 is applied). Corresponding snapshots (d), (e), (f), all taken at t=1.1s after the reentry is formed, show that the diastolic gap (i.e., head-to-tail gap) becomes shorter as the conductivity of the isthmus (calculated relative to that of normal myocardium) increases. Consequently, the resulting VT cycle length is increasing with decreasing electrical conductivity of the isthmus. A plot of VT cycle length vs. the inverse of the square root of the conductivity of isthmus yielded a linear fit with a correlation coefficient of 0.99.

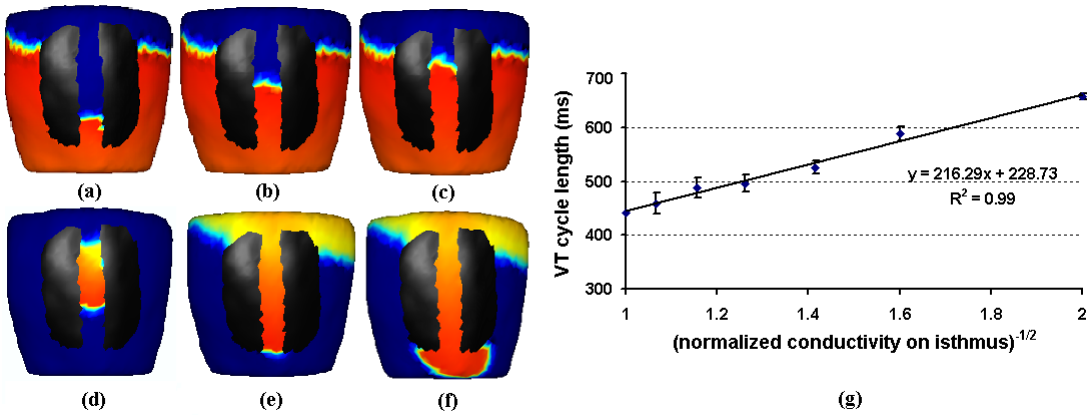

Figure 7. *The effect of conductivity on the VT cycle length: (a-c) comparison between propagations (at t=0.157s after S1 is applied), and (d-f) differences between the diastolic gaps during the reentry (at t=1.1s), when the conductivity in the isthmus is reduced by 75% (a and d), 40% (b and e) and 12% (c and f). A linear fit for VT cycle length vs. the square root of the inverse of conductivity was plotted using Excel (g).*

The effects of tissue anisotropy and fiber directions on the wave propagation are illustrated in Figure 8. For a broader study, we also provide an example where the fibers are all vertical through the ventricular wall (fiber directions for this case are illustrated in Fig 8a).

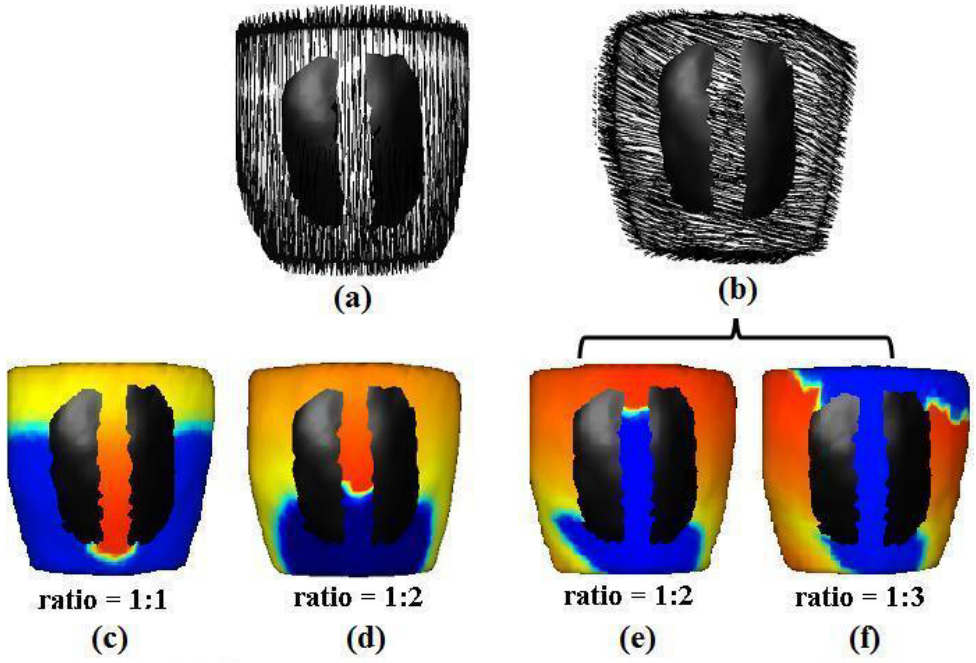

Figure 8. *The effect of fiber direction and anisotropy ratio on the VT cycle length: (a) the vertical fibers and (b) the realistic fibers on the wedge, (c-f) comparison between propagations (at t = 0.764 s) in tissues with different anisotropy ratio, where (d) corresponds to vertical fibers and (c, e-f) correspond to realistic fibers.*

The difference in propagation due to different conduction velocity ratios (CV_{transv} : $CV_{longitud}$) and fiber directions in the representative snapshots are included in Figs 8(c-f), all taken at the same time (i.e., t = 764 ms after the stimulus S1 is applied). Again, ratio=1:1 corresponds to the isotropic case, whereas for conduction velocity ratios of 1:2 and 1:3 the wave travels twice, and three times faster respectively, in the longitudinal direction than it does in the transverse direction. Our results showed that VT cycle length is longer as the conduction velocity across the fibers decreases (in the realistic

fibers case). For instance, the resulting VT cycle length (mean ± SD, calculated for the first three or four reentrant cycles) as a function of the conduction velocity ratio was as follows: 393 ± 18 ms (for the isotropic case), 526 ± 13 ms (for ratio 1:2) and 607 ± 11 ms (for ratio 1:3), respectively. For a ratio of 1:2, in the case of vertical fibers the cycle length is shorter, i.e., VT cycle length was 472 ± 19 ms (mean ± SD).

Figure 9 shows two reentrant circuits formed on the endocardium (note that the infarcts are not transmural). The VT cycle length obtained in the case of "tubular" isthmus (illustrated in Fig. 9b-c) was of 386 ± 15ms. For the thin "sheet-like" isthmus (Fig 9d-e) we obtained a VT cycle length 302 ± 10ms, which was shorter because of the size of scars. Both the thin "sheet-like" and the "tubular" isthmuses have equal cross-section areas of 12 mm^2. However, the thin isthmus has a surface area of 1.9 cm^2 as measured on the endocardium, whereas the area of the left scar adjacent to the thin isthmus is of 1.5 cm^2 which is smaller than the other endocardial reentry scar (i.e., 2.4 cm^2).

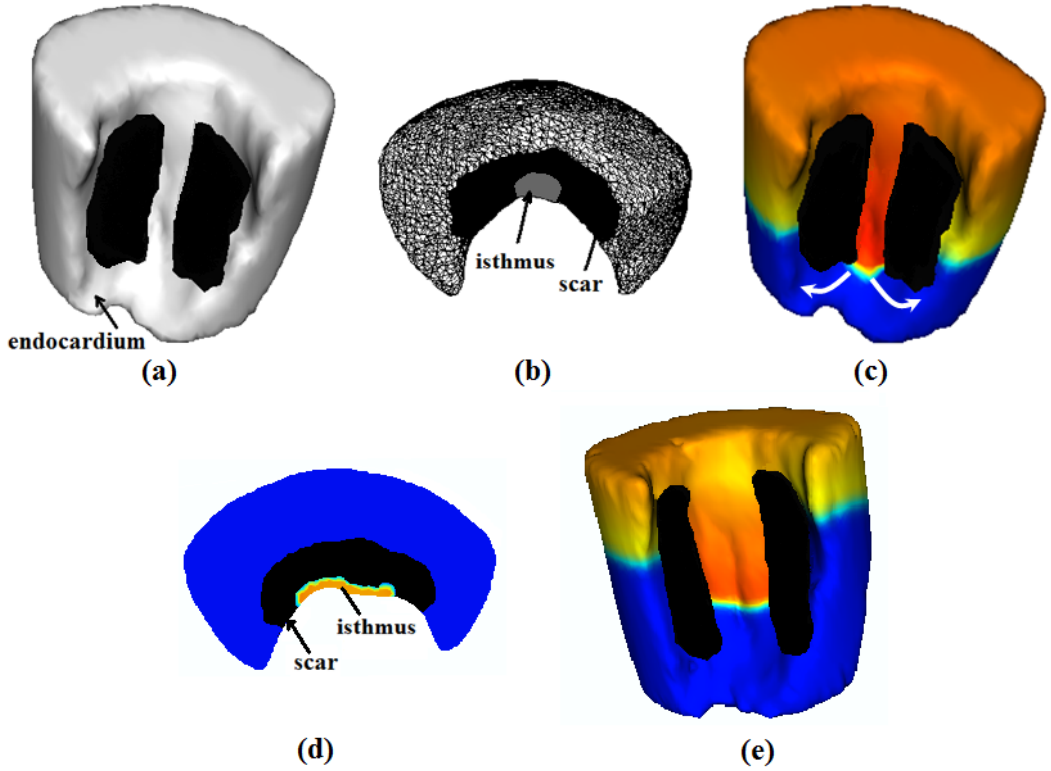

Figure 9. *Example of endocardial reentry: (a) the 3D wedge model with the scars defined on the endocardium; (b) cross-section plane through the mesh corresponding to "tubular" isthmus; (c) propagation of the reentrant wave around the scars, with the depolarization wave front (in red) exiting the isthmus (and further propagating in the directions shown by the white arrows); (d) cross-section plane through the wedge with thin "sheet-like" isthmus and (e) corresponding propagation of the reentrant wave through the thin isthmus.*

3.3. The effect of RFA lesions and changes in scar geometry on VT cycle length

We present two different cases where the changes in scar geometry affect the VT cycle length due to changes in: (i) cross-section area of the isthmus, and (ii) the total path length.

In the first case, we simulated RF therapy by introducing ablation lesions (of zero conductivity) at different sites relative to the isthmus. Placing one small RF lesion at the exit of the isthmus (see figure 10a-b) had no effect on VT inducibility or the cycle length; this gap in the lesion allowed the reentrant wave to escape and to continue looping around the scars. Obviously, the reentry was interrupted by placing RF lesions completely across the isthmus (Fig 10c-d). However, we noted that after placing more lesions along the length of the isthmus (figure 10e-f) the VT cycle length is increased compared

to that before ablation. For instance when conductivity of isthmus is reduced by 50% and the anisotropy ratio is set to 1:2, cycle length increased from an average of 526 ms prior to ablation to 590 ms after placing lesions all along the length of the isthmus (Fig 10g). The increase was likely due to a decrease in the cross-sectional area of the isthmus (from ~15mm^2 to ~8mm^2), which decelerated the wave through the isthmus.

The time taken by the wave to travel through the outside path (i.e., the healthy myocardium) remained the same as that prior to ablation (~324 ms), whereas the time taken to travel through the isthmus increased by 26% (i.e., from 199 ms to 267 ms) after ablation. Moreover, for the ratio 1:3 (simulation results not included), the wave is considerably decelerated, such that the new VT cycle length is longer than 700 ms (resulting in the annihilation of the reentrant wave by the normal S1-triggered wave).

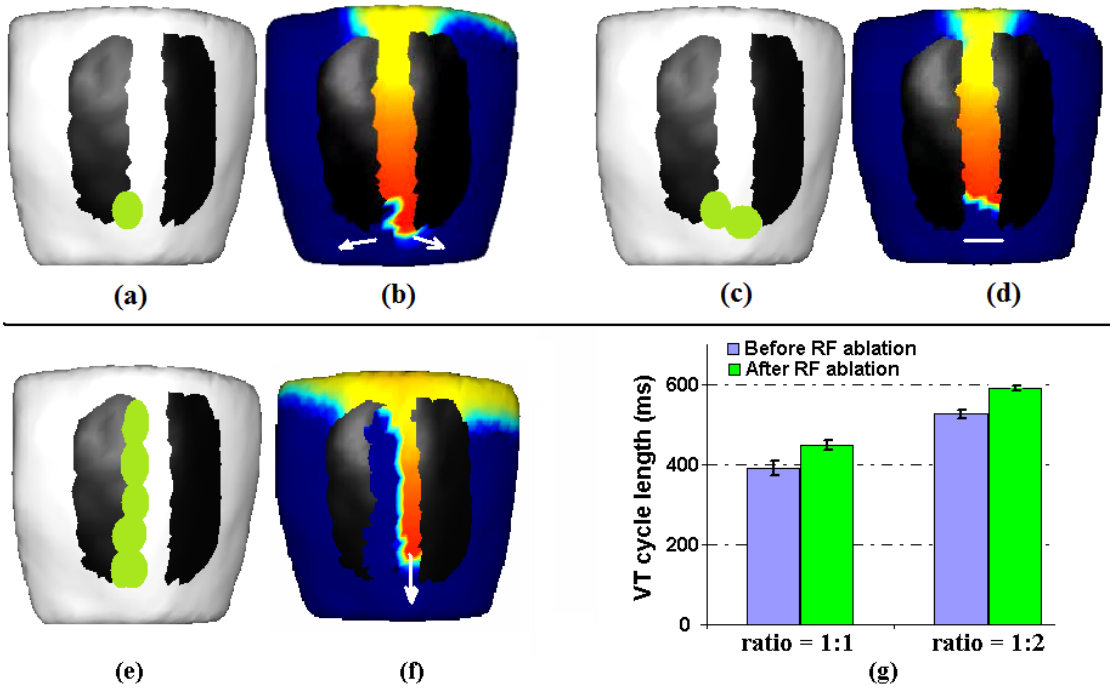

Figure 10. *Re-inducibility of VT after incomplete ablation of the isthmus allowing the wave to escape through the gap (a-b); non-inducibility of VT after complete ablation of the isthmus (c-d); multiple RF lesions placed along the isthmus results in wave deceleration and an increase in VT cycle length, for the case presented in (e-f).*

Figure 11 presents the other simulated case, in which we modified the scar geometry by introducing a second isthmus (i.e., a bystander) within the scar (Fig 11a). The bystander is "silent" (i.e., has no effect) during the normal propagation and inducibility of VT (Fig 11b). After complete ablation of the principal isthmus, the VT is re-inducible and the wave travels around the scars through both paths [1] and [2], as seen in Fig 11c. The resulting reentrant wave propagated through the bystander and looped around the scar via the shorter path (i.e., path 1 in Fig 11c). A shortening in the cycle length (i.e., from 526 ms to 487 ms) is observed when the wave goes through the bystander for the case where the anisotropy ratio was set to 1:2.

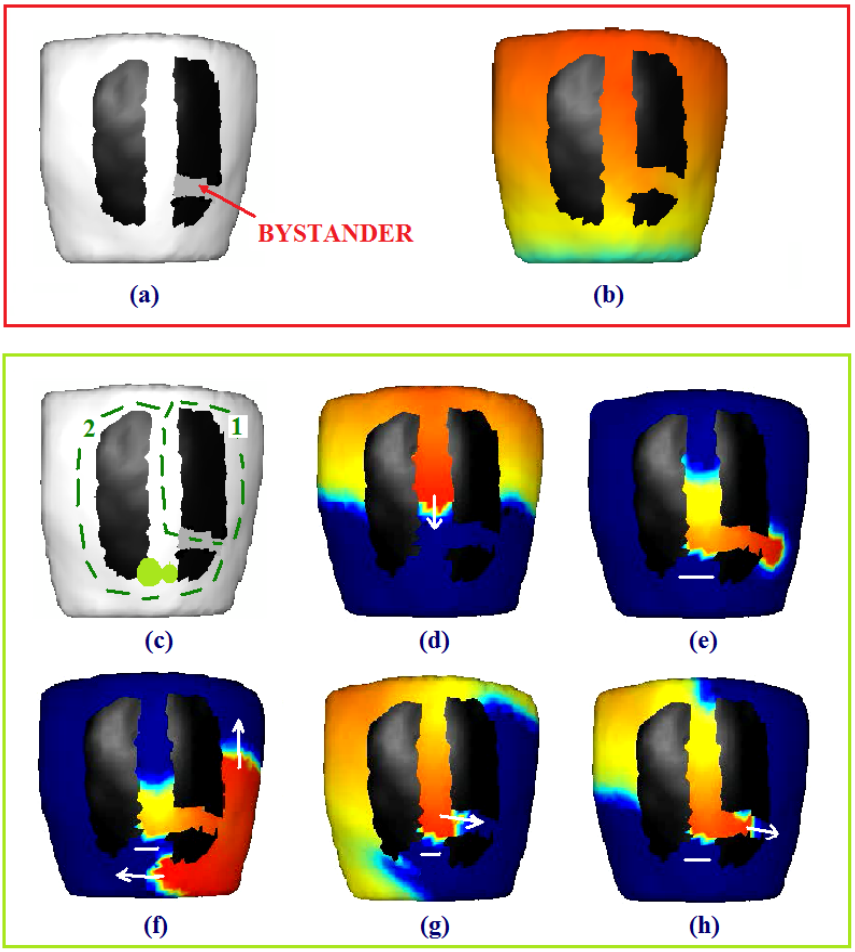

Figure 11. *VT re-inducibility in the presence of a bystander: (a) scar with main isthmus and bystander (b) propagation of wave prior ablation (red panel) and (c-h) re-inducibility of VT after ablating the main isthmus (green panel). In (c) the green areas denote the RFA lesions and the green dash lines delineate the paths for the excitation wave.*

4. Discussion

The aim of this work was to develop a simple 3D theoretical model that captures the electrophysiology phenomena associated with some specific morpho-pathological changes in a post-infarct heart. We sought to investigate the propagation of electrical waves in the presence of anatomic reentry generated by abnormal circuits comprised of chronic scars and isthmuses of viable tissue bundles. For this disease, of clinical relevance are the inducibility of VT as well as the VT cycle length in patients with prior myocardial infarction; these characteristics are ultimately associated with risk of sudden cardiac death. For clinical applications, it is important to use a fast mathematical model with attractive computational times, like the Aliev-Panfilov monodomain model (adapted from reaction-diffusion FitzHugh-Nagumo model), so that different conditions can be reviewed for a given patient. In our study, it takes about 1h on one standard PC (e.g. Intel ® Pentium 4, 3.2GHz CPU, with 1GB of RAM) to simulate 1s of a heart cycle, compared to 2h for 1s of heart cycle simulated with the Luo-Rudy model using thirty 1.4GHz processors in parallel [Xie *et al.*, 2004] or 2 days with the bidomain model [Potse *et al.*, 2006] on 32 processors. The latter study demonstrated that the propagations of AP were only 2% faster in the bidomain model than in the monodomain model, the latter solving for the transmembrane voltage without knowledge about the individual ionic currents and concentrations; this justifies our choice of (monodomain) model.

In the current work, we first used our 3D mathematical model to study the conditions favoring the inducibility of unidirectional block (UB) and its associated vulnerable window. The width of the VW (as defined by its lower and upper limits), was found to strongly depend on the isthmus conductivity

and myocardial anisotropy. The width of VW (obtained by gradually reducing the S1-S2 interval) increased as the conductivity in the isthmus decreased. As per the CV restitution curve (appendix, Fig A1d), as the S1-S2 interval decreases, so does the CV; thus when S2 lies in the recovery tail of S1, the action potential cannot be elicited. Healthy tissue (beneath the stimulus S2) recovers before the isthmus, explaining the lower limit of VW. In general, a reduction in the value of isthmus conductivity triggers a delay of the wave propagation through the isthmus; thus the time when the S2 can actually depolarize again the isthmus (upper limit of VW) increases. Similar findings were provided in [Ten Tusscher and Panfilov, 2007], where the reduction in conductivity was specifically attributed to increased diffuse fibrosis (a major cause of cellular uncoupling). Specifically, in their modelling study, these authors obtained a variation in VW reflected in increasing size of very small, randomly distributed obstacles.

In our study, we also found that the VW width increased by three times as the anisotropy ratio of the myocardium was set to 0.11 compared to the isotropic case (ratio = 1). This suggests that fiber directions should always be included in calculations to avoid erroneous estimates. The upper limit of the VW remained almost constant for anisotropy ratios greater than 0.25. This behaviour is due to the speed of the depolarization wave relative to the position of the S2 stimulus at the entrance of the isthmus, and to the fiber orientation in the isthmus. As the local anisotropy is increased (i.e., the transverse CV is reduced) the wave front will move slower through the isthmus; thus an effect similar to the reduction of conductivity was obtained (given that the fibers are not parallel with the isthmus axis, but rather at an angle). More generally, we calculated the S1-S2 interval at a selected location (i.e., node in the mesh) in the middle of the small area where S2 is applied. Therefore, for each lower/upper limit of the unidirectional block (UB), we subtracted the time required for the wave to travel from the bottom of the wedge (where S1 is applied) to that certain point. In the case where we kept the anisotropy constant and varied the conductivity in the isthmus (illustrated in Fig 6a), this time is the same for all simulations. In the case where we varied the anisotropy ratio (Fig. 6b), this time is not the same but rather increases as the ratio is decreased from 1:1 to1:3; therefore the lower limit for unidirectional block shifts to earlier times. Thus, for the particular case we modelled, changes in conductivity of isthmus reflect local effects, whereas changes in anisotropy reflect global effects on the UB.

Once induced, the reentrant wave circulates around the scars and enters the circuit from the other end of the isthmus. That is because this region of tissue (i.e., “the entrance”) has already recovered and is excitable, in accordance with many experimental findings and clinical observations, as reviewed in [Kleber and Rudy 2004]. The VT cycle length is known to depend on tissue conduction velocity and the path length, the latter being actually the perimeter of the obstacles; the results from our study are in accordance with these observations. The circuit dimensions (scar and isthmus) and the electrical properties of the isthmus set the vulnerable window in which the VT can be induced. However, it is very difficult to analytically calculate the VT cycle length due to the fact that realistic scars are irregular in shape and the fiber orientation varies along the boundaries. Our results show that VT cycle length is longer in the case where the fibers were oriented at an angle to the axis of the isthmus, compared to the case where fibers are parallel; this result is consistent with experimental observations in a canine model of reentry [Ciaccio *et al.,* 2001]. Moreover, while the speed of the activation front may be constant within the middle portion of the isthmus, the exit and the entrance introduce deceleration and acceleration. Given these issues, simulations should yield more accurate estimates of CV, thus can be used as a tool to help the clinician estimate VT inducibility and an expected cycle length. With this respect, macro-reentries of clinical relevance have dimensions on the order of a few cm [Soejima *et al.,* 2001 and 2002; Ciaccio *et al.,* 2001; Chillou *et al.,* 2002]. This is due to the fact that the wave front has to rotate around the circuit in a time that is longer than the duration of the previous action potential (otherwise the head of the wave will reach the refractory tail). The perimeter of the non-conductive scars sets the physical distance that the wave has to travel in order to circumscribe completely the conduction block(s). However, the excitation wave travels through different segments of the reentrant circuit (i.e. healthy tissue, isthmus) at different conduction velocities.

Experimental and computational studies have already suggested that the conduction velocity is affected by tissue conductivity and the radius of narrow paths. Particularly, with respect to the dimensions of the narrow paths (like isthmuses), it was showed in [Kogan *et al.,* 1992] using 2D simulation studies, that the width of the narrow path (i.e., isthmus) is critical to the conduction velocity; notably, the wave propagates slower as the diffusion coefficient d in the isthmus decreases, and later in [Bub and Shrier, 2002] that the propagation will be blocked below a critical width of the isthmus at its exit, creating a source-sink mismatch. Another recent simulation study demonstrated that the radius of

a narrow channel traversing a rectangular slab of tissue (with fibers parallel to the axis of the channel and different degrees of uncoupling between ischemic and normal myocardium) contributes to the inducibility of reentry in the phase B of acute ischemia [Jie *et al.*; 2008]. We found a similar result in our previous study [Pop *et al.,* 2008]; however, we suggested that this is also due to the current consumption at the boundary between infarct and isthmus. In the current study, this was again noted in the case where we changed the dimensions of the isthmus by placing RF lesions along it, reducing by almost half the cross-sectional area of the isthmus. This is also probably due to the partial-flux boundary condition between the scars and the isthmus, allowing some consumption of current at the interface between these two zones. As expected, an increase in VT cycle length observed following placement of RF lesions on the isthmus. As a consequence, VT cycle length increased; specifically, we saw a 23% increase when the conduction velocity ratio was set to 1:2.

The presence of a small gap in the ablated lesion favors the re-inducibility of VT following therapy [Kottkamp *et al.,* 2003]. However, there is clinical evidence showing that the RF lesions cause a "stricture" in the isthmus and decelerate the propagation of the wave [Ellison *et al.,* 1998]. Our simulation results reflect this clinical observation and demonstrate that, while the VT may be re-inducible in such cases, the actual VT cycle length can be increased after introducing the non-conductive RF lesions. Although the new VT is less dangerous (cycle length is longer), it is still not terminated. The reentry was stopped when the conduction velocity ratio was set to 1:3 (i.e., anisotropy ratio is 0.11), which resulted in a very slow propagation through the isthmus. In this case, the wave was decelerated so that the next wave from stimulus S1 annihilated the reentrant wave. The model can thus help the clinician to test ablation strategies. Our results suggest that the ablation where the lesions are placed completely across the isthmus is more efficient than lesion placement all along the isthmus. An unidentified bystander for one VT can become the critical isthmus for another circuit; thus identification of all small channels is desirable prior to ablation. One could target the exit and the entrance of the principal isthmus, because this would interrupt the potential breakthrough of the wave through the bystander. In practice, clinicians often place RF lesions all along the boundaries of the infarct, which is time consuming; thus the potential isthmuses should be identified via an imaging technique and a model should be built based on such anatomical findings to reduce procedure duration.

Computationally fast models of cardiac activity could be integrated into clinical EP applications and used to predict the propagation of electrical waves in the heart, and to assess the inducibility of VT before and following the RF therapy. Such models could also be used as aids for designing more robust ablation treatments, by identifying patterns less sensitive to ablation location. The ultimate clinical goal is to increase the procedure efficacy, shorten the procedure time and avoid further impairment of ventricular function. This important "translation to clinic" step requires not only realistic identification of infarct scars from MR data and extension to a full 3D anatomic model of the heart, but also experimental validation [Ciaccio *et al.,* 2007]. Image-based models are currently being developed; high-resolution anatomical models of the rabbit and canine heart are available to explore genesis of and propagation patterns in scar-related arrhythmias [Vigmond *et al.,* 2009]. Our recent efforts were focused on successfully developing a similar 3D cardiac imaged-based computational model from DW-MRI in infarcted porcine hearts [Pop *et al.,* 2009b].

Study limitations

The two-variable model proposed by FitzHugh and Nagumo, and later improved by Aliev and Panfilov, although very attractive because it is fast (compared to ionic and bidomain models) has certain drawbacks. The monodomain formalism is based on the assumption that intra- and extracellular spaces are "collapsed" into each other; thus they are represented by the same conductivity value. In reality, these two cellular spaces have distinct conductivity values. The voltage solution has normalized values (between 0 and 1), instead of realistic values in the range -90ms and 20ms which can be measured experimentally.

Regarding the model parameters associated with the action potential wave, in the current paper, we modelled the excitability of the isthmus and the healthy myocardium using constant values for the parameter *k*; some experimental studies reported that the isthmus might have reduced excitability. In another simulation study [Vigmond *et al*.; 2009] the border zone (i.e., the peri-infarct area) was modelled with a longer action potential duration (APD) and reduced excitability relative to the normal myocardium. Indeed, such changes are known to be very important in the acute and sub-acute ischemic phases of the infarct; for instance, the APD is known to slowly recover within the first

weeks during healing (i.e., the sub-acute phase) and to return to values close to the baseline (healthy myocardioum). Specifically, AP of the cells in the border zone was noted to have longer duration than in healthy myocardium at two months after infarction (Ursell *et al.*, 1985). However, an optical study in an infarct rat model has shown that there is no significant change in the APD values between the border-zone and remote/healthy tissue [Mills *el al.*; 2005]. Since our reentry circuit was artificially created, we have not included such regional changes in the APD, which would affect the recovery time of the isthmus, and consequently, the vulnerability window.

During the infarct healing in the chronic phase of the disease, the fiber directions change in the isthmus due to the deposition of collagen, which generates a slower and more 'tortuous' propagation through the isthmus compared to the simplified case we modeled. Thus, a real isthmus is not a "homogeneous entity" with constant parameters but has segments of different conductivity values as well as fiber disarray and altered architecture that would contribute to different local speeds of propagation; in particular, the transverse component of the speed is reduced more dramatically, as reviewed in several seminal studies [Janse and Wit, 1989; De Bakker *et al.*, 1988].

Finally, the geometrical model (i.e., the specific pattern that we used) represents the typical clinical case with one central isthmus, which is more commonly the target for RF ablation and two large scars (as presented in Fig.1). However, these two scars could have different perimeters (the smaller scar driving the VT cycle length) and might also have various geometries due to different locations within the territory of other major vessels; such cases cannot be appropriately studied using a simplified wedge model.

5. Conclusion

To conclude, we have developed a 3D computer model that predicts the inducibility of VT associated with anatomic reentry around infarct scars. Via computer simulations of cardiac electrical activity, we studied the physical conditions favoring the inducibility of reentrant VT and found that the isthmus conductivity and tissue anisotropy are critical to the induction of UB, the initiation of the reentrant wave and the VT cycle length. RF ablation lesions placed on the isthmus can interrupt or modify the VT cycle length.

Acknowledgements

The authors would like to thank Dr. Yves Coudière, Dr. Michael Bronskill and Dr. Michael Kolios for helpful discussions. Mihaela Pop was supported from a Heart and Stroke of Canada doctoral research award while the research work was supported by the Canadian Institutes of Health Research grant (MOP93531).

Appendix

The restitution curves for action potential and conduction velocity

The action potential duration (APD) and the local conduction velocity CV change with the pacing stimulus interval (described as cycle length, CL); which in turn determines the diastolic interval, DI. This property is named *restitution* and characterizes the dynamic response of the cardiac tissue at different cycle lengths, where CL is the sum between APD and DI. The restitution curves relate APD and CV to the preceding DI of a cycle and can be characterized by the following relationships:

$$APD_n = f(DI_{n-1}) = f(CL_{n-1} - APD_{n-1}) \quad \text{(A1)}$$

$$\text{and } CV = g(DI_{n-1}) \quad \text{(A2)}$$

where: *n* denotes a particular cycle beat.

Both curves can be measured in simulations using different pacing protocols. In our simulations we paced homogeneous tissue at constant S1-S1 intervals of 830 ms followed by a stimulus S2. To avoid erroneous estimates of CV that could be introduced by the curvature of the realistic wedge, S1 and S2 were delivered at the bottom of a rectangular slab (the same one that was used in [Pop *et al.*, 2008a]), but with no heterogeneities in terms of zones and tissue properties. The coupling interval S1-S2 was reduced until no propagation of AP could be generated. We performed all the calculations as per the methodology provided in [Clayton and Holden; 2003] except that in their study they paced at a S1-S1 interval of 50 0ms.

For the action potential restitution curve, the APD_{90} (APD at 90% repolarization, which is 0.9 times the difference between the APD's peak amplitude and the baseline) was calculated (e.g. APD_{90} is 320ms for S1-S2=700 ms). The APD_{90} and the CV were measured in the centre of the rectangular slab and plotted against the preceding DI interval. From the APD_{90} restitution curve (figure A1c) we observe that the function in equation (A1) is exponential, whereas, in the conduction velocity restitution curve, CV is constant for large diastolic intervals but decreases abruptly as the DI decreases to values lower than 100 ms (see figure A1d).

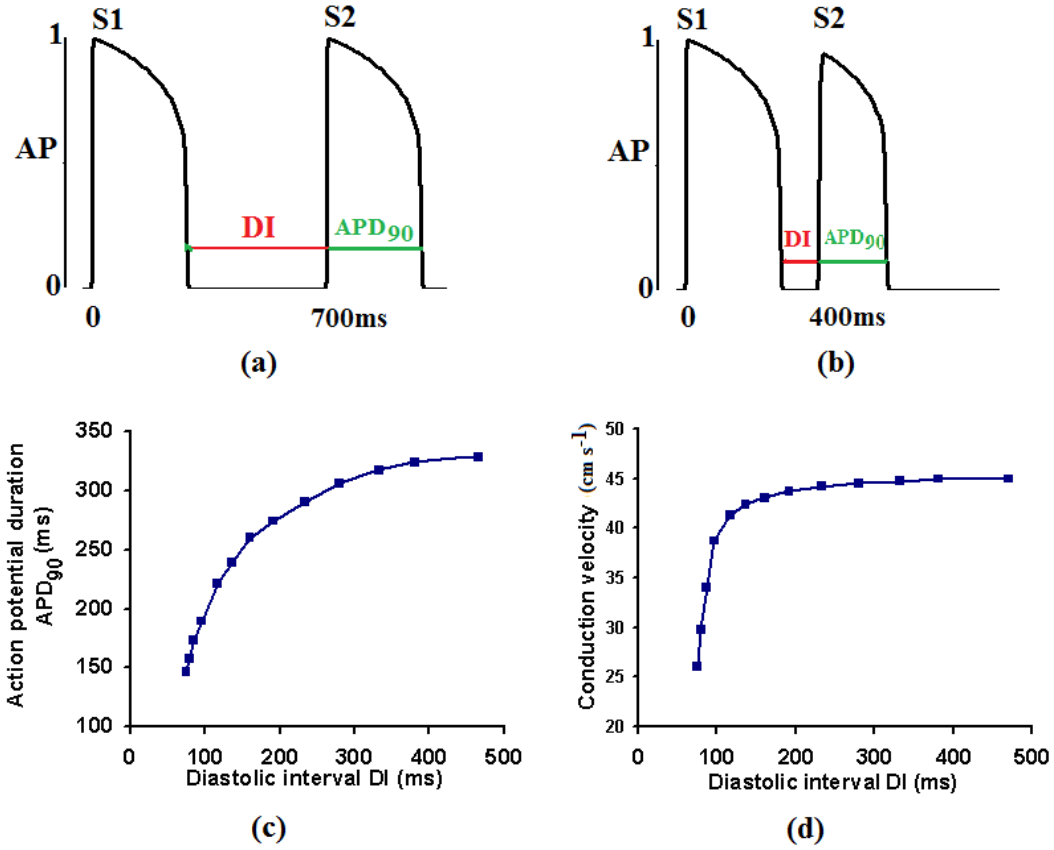

Figure A1 *Traces of AP obtained by pacing at basic cycle (defined by the S1-S1 interval) and gradually reducing the coupling interval S1-S2 until an electrical excitation could not be elicited (a-b); corresponding restitution curves for action potential duration (c) and conduction velocity (d) as a function of DI.*

References:

Aliev R and Panfilov A V A simple two-variables model of cardiac excitation *Chaos, Soliton and Fractals* 7 293-301 1996a

Aliev R and Panfilov A V Modeling of heart excitation patterns caused by local inhomogeneities *Journal of Theoretical Biology* 181 33-40 1996b

Benson AO, Ries ME and Holden AV Effects of geometry and architecture on re-entrant scroll wave dynamics in human virtual ventricular tissues Proceedings of FIMH 2007 (Springer-Verlag Berlin Heidelberg), *LNCS* 4466 pp200-209, 2007

Bernus O, Verschelde H and Panfilov A V Modified ionic models of cardiac tissue for efficient large scale computations *Physics in Medicine and Biology* 47 1947-1959, 2002

Bolick D R, Hackel D B, Reimer KA, Ideker R E Quantitative analysis of myocardial infarct structure in patients with ventricular tachycardia *Circulation* 74 1266-1279, 1986

Bub G and Shrier A Propagation through heterogeneous substrates in simple excitable media model *Chaos* 12 747-753, 2002

Ciaccio E J, Costeas C, Coromilas J, Wit AL Static relationship of cycle length to reentrant circuit geometry *Circulation* 104 1946-195, 2001

Ciaccio E J, Tosti A C, Scheinman M Method to predict isthmus location in ventricular tachycardia caused by reentry with double loop pattern *Journal of Cardiovascular Electrophysiology* 14 528-536, 2003

Ciaccio E J, Ashikaga H, Kaba R A, Cernantes D, Hopenfeld B, Wit A L, Peters N S, McVeigh E R, Garan H, Coromils J Model of reentrant VT based on infarct border zone geometry predicts reentrant circuit features as determined by activation mapping *Heart Rhythm.* 4 1034-45, 2007

Clayton R H Computational models of normal and abnormal action potential propagation in cardiac tissue: linking experimental and clinical cardiology *Physiol. Meas.* 22 R15-R34 2001

Clayton R H and Holden A Effect of regional differences in cardiac cellular electrophysiology on the stability of ventricular arrhythmias: a computational study *Phys. Med. Biol.* 48 95-111, 2003

Clayton RH and Panfilov AV A guide to modelling cardiac electrical activity in anatomically detailed ventricles *Prog Biophys Mol Biol* 96 (1-3) 19-43, 2008

De Bakker JMT, Van Capelle FJL, Janse MJ, Wilde AAM, Coronel R, Becker AE, Dingemans KP, Van Hemel NM , Hauer RNW Reentry as a cause of VT in patients with chronic ischemic heart disease: electrophysiologic and anatomic correlation *Circulation*, 77(3) 1988

De Chillou C, Lacroix D, Klug D, Magnin-Poull I, Marquié C, Andronache M, Kouakam C, Sadoul N, Chen J C, Aliot E, Kacet S Isthmus characteristics of reentrant VT after myocardial infarction *Circulation*, 105 726-731, 2002

Durrer D, van Dam R T, Freud G E, Janse M J, Meijler F L, Arzbaecher R C Total excitation of the isolated human heart *Circulation* 4 899-912, 1970

Elharrar V and Surawicz B Cycle length effect on restitution of action potential duration in dog cardiac fibers *Am. J. Physiol.* 244 H782–H792, 1983

Ellison K E, Friedman P L, Ganz L I, *et al.*, Entrainment mapping and radiofrequency ablation of VT in right ventricular dysplasia. *J Am Coll Cardiol* 32 724-728, 1998

FitzHugh R A Impulses and physiological states in theoretical models of nerve membrane *Biophysical Journal* 1 445-466, 1961

Friedman M, Ovsyshcher IE, Fleidervish I, Crystal E and Rabinovich A: Stimulation of unidirectional pulses in excitable systems *Physical Review E (Stat Nonlin Soft Matter Phys)* 2004, 70 (4 Pt 1): 041903

Garrat C Mechanism and management of cardiac arrhythmias. Blackwell, British Medical Journal, 2001

Girouard ST and Rosenbaum DS Role of wavelength adaptation in the initiation, maintenance and pharmacological suppression of reentry *Journal of Cardiovascular Electrophysiology* 12 697-707, 2001

Huikuri H, Castellanos A, Myerburg R Sudden death due to cardiac arrhythmias *New England Journal of Medicine* 345 1473-1482, 2001

Janse M J and Wit A L Electrophysiological mechanisms of ventricular arrhythmias resulting from myocardial ischemia and infarction *Physiological Review* 69 1049-1169, 1989

Jie X, Rodriguez B, De Groot JR, Coronel R, Trayanova N Reentry in survived subepicardium coupled to depolarized and inexcitable midmyocardium: Insights into arrhythmogenesis in ischemia phase 1B *Heart Rhythm* 5 1036-1044, 2008

Kawara T, Derksen R, De Groot J R, Coronel R, Tasseron S, Linnenbank AC, Hauer R N, Kirkels H, Janse M J, De Bakker J M T Activation delay after premature stimulation in chronically diseased human myocardium relates to the architecture of interstitial fibrosis *Circulation* 104 3069-3074, 2001

Kleber AG and Rudy Y Basic mechanisms of cardiac impulse propagation and associated arrhythmias *Physiological Review* 84, 431-488, 2004

Kogan B, Karplus, Billet BS, Stevenson WG Excitation wave propagation within narrow pathways: geometric configuration facilitating unidirectional block and reentry *Physica D* 59 275-296, 1992

Kottkamp H, Wetzel U, Schirdewahn P, Schierdewahn P, Dorszewski A, Gerds Li J H, Carbucicchio C, Kobza R, Hindricks G Catheter ablation of ventricular tachycardia in remote myocardial infarction: substrate description guiding placement of individual linear lesions targeting non-inducibility *Journal of Cardiovascular Electrophysiology* 14 675-681, 2003

Krogh-Madsen T and Christini DJ: Resetting and termination of reentry in a loop-and-tail cardiac model. *Physical Review E (Stat Nonlin Soft Matter Phys)* 77 (1 Pt 1): 011916, 2008

Luo C and Rudy Y A dynamic model of the cardiac ventricular action potential: Simulations of ionic currents and concentration changes. *Circulation Research* 74 1071–1096, 1994

Martinez-Rubio A, Bayes-Genis A, Guindo J, Bayes de Luna A Sudden cardiac death *Contributions to Science* 1 147-157, 1999

Mills WR, Mal N, Forudi F, Popovic ZB, Penn MS, Laurita KR Optical mapping of late myocardial infarctions in rats *Am J Heart Circ Physiol* (290) H1298-1306, 2005

Nagumo J, Arimoto S, Yoshizawa An active transmission line simulating nerve axon *Proceeding of the I.R.E.* 50 2061-2070, 1962

Nash MP and Panfilov AV, Electromechanical model of excitable tissue to study re-entrant cardiac arrhythmias *Progress in Biophysics and Molecular Biology* (85) 501-522, 2004

Noble D A modification of the Hodgkin–Huxley equation applicable to Purkinje fiber action and pacemaker potentials. *Journal of Physiology* (160) 317–352, 1962

Schmidt A, Azevezo C F, Cheng A, Sandeep N G, Bluemke D A, Foo T K, Gerstenblith G, Weiss R G, Marban E, Tomaselli G F, Lima J A C, Wu KC Infarct tissue heterogeneity by magnetic resonance imaging identifies enhanced cardiac arrhythmias susceptibility in patients with left ventricular dysfunction *Circulation* 115 (e-pub April 9) 2007

Sermesant M, Faris O, Evans F, McVeigh RH, Coudiere Y, Delingette H, Ayache Y Preliminary validation using in vivo measures of a macroscopic electrical model of the heart *Int. Symp. on Surgery Sim. & Tissue Modelling* vol. 2673. Springer-Verlag, 230-243, 2003

Sermesant M, Rhode K, Hegde S, Sanchez-Ortiz G, Rueckert D, Lambiase P, Bucknall C, Hill D, Razavi R Simulation of the electromechanical biventricular model using XMR interventional imaging *Medical Image Analysis* 9 (5) 467-80, 2005

Sermesant M, Delingette H, Ayache N: Electromechanical modelling of the heart for medical image analysis and simulation *IEEE Transactions in Medical Imaging* 25 612-625, 2006

Sinha S, Stein K, Christini D Critical role of inhomogeneities in pacing termination of cardiac reentry *Chaos* 12 893-901, 2002a

Sinha S and Christini D Termination of reentry in an inhomogeneous ring of model cardiac cells *Phys Rev E Stat Nonlin Soft Matter Phys* Dec 66(6 Pt 1): 061903, 2002b

Soejima K, Suzuki M, Maisel WH, Sapp JL, *et al*., Catheter ablation in patients with multiple and unstable ventricular tachycardias after myocardial infarction: short ablation lines guided by reentry circuit isthmuses and sinus rhythm mapping. *Circulation* 104 664-669, 2001

Soejima K, Stevenson WG, Maisel WH, Sapp JL, Epstein LM Electrically unexcitable scar mapping based on pacing threshold for identification of the reentry circuit isthmus. Feasibility for guiding VT ablation. *Circulation* 106 1678-1683, 2002

Stevenson WG, Khan H, sager P, Saxon LA, Middlekauff HR, Natterson PD, Wiener I Identification of reentry circuit sites during catheter mapping and RF ablation of ventricular tachycardia late after myocardial infarction *Circulation* 88 1647-1670, 1993

Stevenson WG, Nademanee K, Weiss JN, Wiener I, Baron K, Yeatman LA, Sherman CT Programmed electrical stimulation at potential ventricular reentry circuits sites. Comparison of observations in humans with predictions from computer simulations *Circulation* 80 793-806, 1989

Panfilov AV Spiral breakup in an array of coupled cells: the role of intercellular conductance *Physical Review Letters* 88: 118101, 2002

Peters NS and Wit AL Myocardial architecture and ventricular arrhythmogenesis *Circulation* 97: 1746-1754, 1998

Pogwizd SM, Hoyt RH, Saffitz JE, Corr PB, Cox JJ, Cain ME Reentrant and focal mechanisms underlying ventricular tachycardia in human heart *Circulation* 86: 1872-96, 1992

Pop M, Sermesant M, Dick AJ, Coudiere Y, Wright GA Modelling anatomic reentry - a 3D study on a virtual slab *Proceeding of Modelling and Simulation IASTED* MS, Quebec City, May 26-28, Acta Press, 620-162, 2008

Pop M, Sermesant M, Lepiller D, Truong MV, McVeigh ER, Crystal E, Dick AJ, Delingete H, Ayache N, Wright GA Fusion of optical imaging and MRI for the evaluation and adjustment of macroscopic models of cardiac electrophysiology: a feasibility study *Medical Image Analysis* Apr; 13(2):370-80, 2009a

Pop M, Sermesant M, Mansi T, Crystal E, Detsky JS, Yang Y, Fefer P, McVeigh ER, Dick AJ, Ayache N, Wright GA Characterization of porcine infarcts heart: insights from experiments and theoretical modelling (Proceedings of the FIMH, June 3-5 2009, Nice) *LNCS* vol 5528: 1-10, (Springer-Verlag Berlin Heidelberg), 2009b

Potse M, Dube B, Richer J, Vinet A, Gulrajani RM A comparison of monodomain and bidomain reaction-diffusion models for action potential propagation in human heart *IEEE Transactions in Biomedical Engineering* 53 2425-35, 2006

Ten Tusscher KHWJ and Panfilov AV Influence of non-excitable cells on spiral breakup in two-dimensional and three-dimensional excitable media *Phys Rev Stat Nonlin Soft Matter Phys* 68 062902, 2003

Ten Tusscher KHWJ and Panfilov AV Wave propagation in excitable media with randomly distributed obstacles *Multiscale Modelling and Simulation* 3; 265-282, 2005

Ten Tusscher KHWJ and Panfilov AV Influence of diffuse fibrosis on wave propagation in human ventricular tissue *Europace* 9; 38-45, 2007

Trayanova N Defibrillation of the heart: Insights into mechanism from modelling studies *Experimental Physiology* 91; 323-327 2006

Ursell PC, Gardner PI, Albala A, Fenoglio JJ and Wit AL Structural and electrophysiological changes in the epicardial zone of canine myocardial infarcts during infarcts healing *Circulation Research* 56; 436-451, 1985

Vigmond E, Vadakkumpadan D, Gurev V, Deo M, Plank G, Trayanova N Towards predictive modelling of the electrophysiology of the heart *Experimental Physiology* 94 562-77, 2009

Weiser L, Fischer G, Hintringer F, Ho SY, and Tilg B Reentry anchoring at a pair of pulmonary vein ostia – published in *FIMH*, ser. LNCS, no. 3504. Springer, 183-193, 2005

Xie F, Qu Z, Yang J, Baher A, Weiss JN, Garfinkel A A simulation study of the effects of cardiac anatomy in ventricular fibrillation *The Journal of Clinical Investigation* 113, 686-693, 2004